Optimal feeding and swimming gaits of biflagellated organisms

Citation: Tam, D., and A. E. Hosoi. "Optimal Feeding and Swimming Gaits of Biflagellated Organisms." Proceedings of the National Academy of Sciences 108, 3 (January 2011): 1001–1006

As Published: http://dx.doi.org/10.1073/pnas.1011185108

Publisher: National Academy of Sciences (U.S.)

Persistent URL: http://hdl.handle.net/1721.1/116447

Version: Final published version: final published article, as it appeared in a journal, conference proceedings, or other formally published context

Optimal feeding and swimming gaits of biflagellated organisms

Daniel Tam[a,1] and A. E. Hosoi[b]

[a]Department of Mathematics, Massachusetts Institute of Technology, Cambridge, MA 02139; and [b]Department of Mechanical Engineering, Massachusetts Institute of Technology, Cambridge, MA 02139

Edited by Jerry P. Gollub, Haverford College, Haverford, PA, and approved November 12, 2010 (received for review July 29, 2010)

Locomotion is widely observed in life at micrometric scales and is exhibited by many eukaryotic unicellular organisms. Motility of such organisms can be achieved through periodic deformations of a tail-like projection called the eukaryotic flagellum. Although the mechanism allowing the flagellum to deform is largely understood, questions related to the functional significance of the observed beating patterns remain unresolved. Here, we focus our attention on the stroke patterns of biflagellated phytoplanktons resembling the green alga *Chlamydomonas*. Such organisms have been widely observed to beat their flagella in two different ways—a breaststroke and an undulatory stroke—both of which are prototypical of general beating patterns observed in eukaryotes. We develop a general optimization procedure to determine the existence of optimal swimming gaits and investigate their functional significance with respect to locomotion and nutrient uptake. Both the undulatory and the breaststroke represent local optima for efficient swimming. With respect to the generation of feeding currents, we found the breaststroke to be optimal and to enhance nutrient uptake significantly, particularly when the organism is immersed in a gradient of nutrients.

optimization | stroke kinematics | low Reynolds number | efficiency

The vast majority of living organisms are found in an astonishing diversity at micrometric scales. Such seemingly simple unicellular organisms interact with their surroundings and exhibit complex dynamic behaviors in order to access resource-rich environments. The ability to locate and take advantage of such favorable environments relies on a rapid chemotactic response (1, 2). In this paper, we investigate the motility of specific microorganisms to address questions related to the functional adaptation, efficiency, and optimization of biolocomotion.

A dominant trait shared by many microorganisms is the prevalence of flagella as motility appendages. The structure of the axoneme, which constitutes the core of the eukaryotic flagellum, is extremely well preserved across the eukaryotic domain. This same structure is found to propel sperm cells and, when several of them beat collectively as cilia, to expel mucus from human lungs. The eukaryotic flagellum has a complex internal "9 + 2" microtubule structure (3), whose elaborate molecular machinery allows the flagellum to induce local bending moments and actively deform its shape. It is noteworthy that these flagella are widely observed to beat in two significantly different ways: undulatory traveling waves that propagate down the flagellum (as exhibited by sperm cells), and so-called "effective recovery" strokes commonly observed in cilia. Because it is possible for organisms to alter and control the waveform along the flagellum, it is of interest to investigate the functional significance of these specific flagellar stroke patterns and their utility with respect to swimming and feeding.

Previous investigations of nutrient transport and hydrodynamics around microorganisms (4–7) considered model swimmers, neglecting the details of the propulsion mechanisms and swimmer geometries. In contrast, we will focus our attention on a biflagellated swimmer, such as green alga *Chlamydomonas*, and consider the hydrodynamics of specific swimming strokes. *Chlamydomonas* was selected as our archetypal organism because it has been well studied and there exists an abundance of experimental data related to motility. For example, recent studies show that the stroke patterns and synchronization of the flagella of *Chlamydomonas* have been associated with a diffusive "run-and-tumble" dynamics (8). Other research indicates that the interactions between the swimming dynamics of *Chlamydomonas* (and other phytoplankton) and a surrounding shear flow can give rise to thin concentrated layers of microorganisms (9).

A remarkable feature of *Chlamydomonas* is that its flagella are observed to beat in both the effective recovery stroke (10, 11) and the undulatory traveling wave (12, 13). The most common stroke, the breaststroke, has the same effective recovery structure as the stroke of cilia. The other stroke, observed in response to a shock of light (12) or an electric stimulation (13), resembles the undulatory beating patterns of uniflagellates. Here, we elucidate the relevance of these two different beating modes and rationalize their function by computing optimal stroke patterns for biflagellated organisms. More precisely, we will examine the relevance of swimming gaits in relation to swimming efficiency and the generation of feeding currents.

Results

We consider a swimmer of a given geometry, inspired by *Chlamydomonas*, which consists of a rigid spherical cell body of radius $R = 5$ μm and two separate flagella of length $L = 12$ μm and radius $r = 0.15$ μm attached at the surface S of the cell (10) (Fig. 1). Varying the ratio between the flagellum and head lengths $L/R = 1.5$–4.0 did not affect our findings and we therefore only present results for this particular representative geometry. The swimmer is immersed in water of density $\rho \approx 10^3$ kg·m^{-3} and dynamic viscosity $\mu \approx 10^{-3}$ kg·m^{-1}·s^{-1} and performs a "stroke" (i.e., a periodic deformation) at a frequency $f \approx 10$–100 Hz (10, 12). The nondimensional parameter governing the hydrodynamics is the Reynolds number (Re). Here $\mathrm{Re} = \rho R^2 f/\mu \approx 10^{-3}$ to 10^{-2}, which is small, signifying that the flow is dominated by viscous effects and governed by Stokes equations,

$$-\nabla p + \mu \nabla^2 \boldsymbol{u} = \boldsymbol{0},$$

where p is the pressure field and $\boldsymbol{u}$ is the incompressible velocity field which satisfies $\nabla \cdot \boldsymbol{u} = 0$.

The swimmer has two distinct flagella, $i = 1, 2$. The kinematics of the periodic deformations are defined by the curvature $\gamma_i(t,s)$ along each separate flagellum i at time t and arclength s along the centerline. These stroke deformations are constrained to remain in the $(\hat{x}, \hat{y})$ plane (Fig. 1). We only consider stroke kinematics that generate no net rotation of the swimmer and for which the flagella do not intersect or penetrate the cell body. The deformations of the flagella generate a fluid flow $\boldsymbol{u}$ as the swimmer moves

Author contributions: D.T. and A.E.H. designed research; D.T. performed research; D.T. and A.E.H. analyzed data; and D.T. and A.E.H. wrote the paper.

The authors declare no conflict of interest.

This article is a PNAS Direct Submission.

[1]To whom correspondence should be addressed. E-mail: dan_tam@mit.edu.

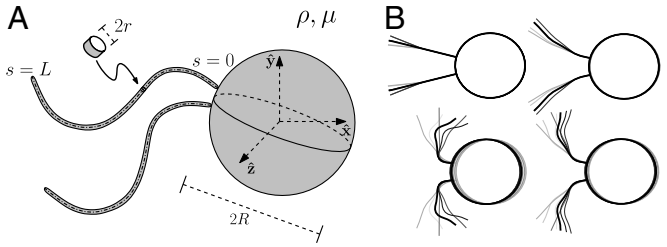

Fig. 1. (*A*) Schematic of the model biflagellated swimmer, relevant length scales and notation. (*B*) Sample of the stroke kinematics used as initial guesses for the optimization procedure.

at an average velocity U in the $\hat{x}$ direction. Both $\boldsymbol{u}$ and U can be computed numerically (see *Methods*). In the following, we motivate the definitions of a swimming and a feeding efficiency, which are then used to optimize the stroke kinematics. Optimal swimming gaits were computed via constrained nonlinear optimization of the curvature functions $\gamma_i(t,s)$ (see *Methods*). To explore the space of all acceptable strokes, optimization procedures were started from a range of initial strokes, a sample of which can be seen in Fig. 1*B*. Note that these initial guesses varied significantly in amplitude and did not resemble any experimentally observed swimming gait.

Optimal Swimming Strokes. The swimming efficiency $\mathscr{E}_s$ is defined as the ratio of the rate of work required to drag the cell body at an average velocity U, to the mechanical power ϕ exerted by the swimmer on the viscous fluid

$$\mathscr{E}_s = \frac{c_0^{\parallel} U^2}{\phi} = \frac{U^2}{U_\phi^2}, \qquad [1]$$

where $c_0^{\parallel} = 6\pi\mu R$ is the axial drag coefficient and U_ϕ the characteristic velocity associated with the mechanical power ϕ, defined such that $\phi = c_0^{\parallel} U_\phi^2$. The definition of $\mathscr{E}_s$ is consistent with previous investigations (14–16) and is a measure of both the speed and energy efficiency of a given stroke. The swimming efficiency, $\mathscr{E}_s$, hence quantifies the hydrodynamic adequacy of a particular stroke for locomotion. Previous studies of optimal strokes for uniflagellated swimmers have suggested the existence of a unique optimal stroke maximizing $\mathscr{E}_s$ (16, 17) consisting of an undulatory traveling wave propagating along the flagellum. Here, we find that the addition of a second flagellum substantially increases the complexity of the optimization problem, resulting in multiple local optima rather than a unique globally optimal solution. These locally optimal strokes are represented in Fig. 2 *A–D*.

Strokes A and B correspond respectively to asymmetric and symmetric undulatory traveling waves, with finite regions of high curvature of alternating signs propagating down the flagellum (Fig. 2 *A* and *B*). Their respective swimming efficiencies are $\mathscr{E}_s^{\mathrm{A}} = 0.0014$ and $\mathscr{E}_s^{\mathrm{B}} = 0.0024$. Stroke C is symmetrical with $\mathscr{E}_s^{\mathrm{C}} = 0.0042$; its structure consists of two regions of high curvature of opposite sign forming simultaneously at the two ends of each flagellum and propagating toward the middle of the flagellum (Fig. 2*C*). Finally, stroke D has the distinctive effective recovery structure of the breaststroke with a finite region of high curvature propagating down the flagellum (Fig. 2*D*). This stroke has the highest swimming efficiency $\mathscr{E}_s^{\mathrm{D}} = 0.0080$.

It is noteworthy that strokes A, B, and D have all been observed in previous experimental studies of living *Chlamydomonas* (8). Fig. 3*A* represents the stroke kinematics of the computed optimal undulatory stroke A, which is in remarkable agreement with experimentally observed undulatory strokes (12) reproduced in Fig. 3*B*.

Optimal Feeding Strokes. Another function of flagellar activity is the generation of feeding currents. Such currents are only relevant if nutrient transport occurs at scales for which advection cannot be neglected with respect to diffusion, as characterized by $\mathrm{Pe} \gtrsim 1$, where Pe is the Péclet number. The velocity-based Péclet number can be expressed in terms of the swimming velocity U, the nutrient diffusivity D, and the radius of the cell R as

$$\mathrm{Pe}^U = \frac{UR}{D}, \qquad [2]$$

and represents the ratio of the swimming velocity to the typical diffusion speed. For *Chlamydomonas* $U \sim 50$–200 μm·s^{-1} (10, 12) and $R \sim 5$ μm. As a green alga, *Chlamydomonas* feeds on inorganic ions (18) but has also demonstrated chemotaxis toward larger organic biomolecules, e.g., maltose and sucrose (19). Considering that *Chlamydomonas* can be found in its natural habitat near freezing temperatures, the nutrient diffusivities range from $D \sim 10^{-10}$ to 10^{-9}m^2.s^{-1} and hence the Péclet number Pe^U varies between ∼0.1 and 10. At these transitional values, diffusion is still a dominant mode of transport but advection also becomes significant and the generation of feeding currents can theoretically enhance nutrient uptake.

Previous studies have investigated the generation of feeding currents using model swimmers with simplified geometries (5, 7, 20), and prescribed deformations (21, 22). Here we consider instead general stroke patterns for our model biflagellate and address questions related to the adaptation, efficiency, and existence of optimal swimming gaits with respect to nutrient uptake. To this end, we define a feeding efficiency $\mathscr{E}_f$—which characterizes how effectively the stroke enhances nutrient uptake—as the fraction of the total energy expense used to create a favorable advective flux of nutrients. To compute this quantity, we require a measure of the flux of nutrients at the surface of the swimmer. Computing the exact nutrient flux requires solving the advection–diffusion equation for the nutrient concentration field which, combined with the optimization procedure, has a crippling computational cost.

We therefore derive an approximate representation of the advective flux by estimating the inbound volumetric flow rate

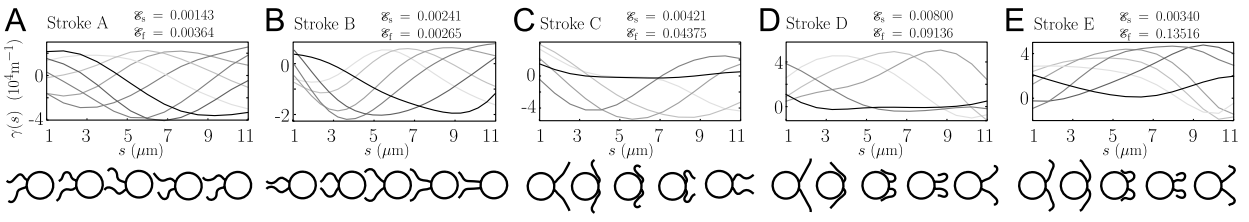

Fig. 2. Representation of the five optimal strokes for biflagellated swimmers computed numerically. Plots represent the curvature γ_i along one flagellum as a function of the arclength at successive times during the strokes. The corresponding stroke kinematics are illustrated by a sequence of shapes, for which all swimmers move to the right. (*A–D*) Strokes A–D are optimized for the swimming efficiency $\mathscr{E}_s$ with initial guess given by (*A*) asymmetric and (*B*) symmetric small amplitude oscillations, (*C* and *D*) large amplitude oscillations. (*E*) Stroke E is optimized for the feeding efficiency $\mathscr{E}_f$ and is found regardless of the initial guess. Values of $\mathscr{E}_s$ and $\mathscr{E}_f$ for each stroke A–E are indicated in the plot.

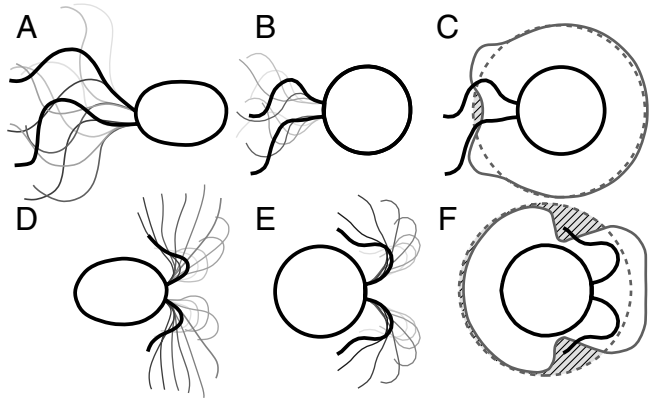

Fig. 3. Comparison between the computed optimal strokes and strokes recorded experimentally. *A–C* correspond to the undulatory stroke and *D–F* to the breaststroke. *A* and *D* represent snapshots of stroke patterns recorded experimentally and are reproduced from refs. 10 and 12. *B* and *E* correspond to snapshots of optimal stroke patterns computed using our procedure. *C* and *F* represent the deformation induced on a closed material line by the undulatory and breaststroke, respectively. The gray dashed line is the circular closed material line of radius $2R$ at the beginning of the stroke and the gray solid line is the corresponding deformed material line at the end of the stroke. The shaded area *A* corresponds to material points dragged closer to the cell surface during the stroke.

over one cycle. Our expression for $\mathscr{E}_f$ relies on the derivation of a characteristic length scale ℓ of fluid displaced by the flagella during one stroke. Because the hydrodynamics are unsteady, the estimation of ℓ cannot rely on averaged flow fields. Instead, exact particle pathlines are integrated in time and ℓ is computed as an averaged displacement of material particles seeded around the swimmer (see *Methods*). Using this length scale, we define the feeding efficiency

$$\mathscr{E}_f = \frac{5\pi\mu\ell(\ell f)^2}{\phi}, \qquad [3]$$

representing the ratio of the power required to move a spherical blob of fluid of radius ℓ at speed ℓf to the total mechanical power ϕ exerted by the swimmer.

Using this definition for $\mathscr{E}_f$ as the new objective function we compute optimal strokes for the generation of feeding currents. We found that regardless of the initial guess (Fig. 1*B*) the procedure converged to a unique optimum, stroke E, represented in Fig. 2*E*. Fig. 3 *D* and *E* illustrate the effective recovery structure of stroke E and highlights the qualitative agreement between our computed stroke E and experimental observations of the breaststroke (10). The feeding efficiency of stroke E is $\mathscr{E}_f = 0.13516$ and is significantly higher than the efficiencies of the swimming strokes A, B, C, and D, whose respective values are $\mathscr{E}_f^{\mathrm{A}} = 0.00354$, $\mathscr{E}_f^{\mathrm{B}} = 0.00265$, $\mathscr{E}_f^{\mathrm{C}} = 0.04375$, and $\mathscr{E}_f^{\mathrm{D}} = 0.04009$. The swimming efficiency of stroke E on the other hand is $\mathscr{E}_s^{\mathrm{E}} = 0.00340$, which is considerably lower than that of the optimal swimming stroke D, $\mathscr{E}_s^{\mathrm{D}} = 0.00801$. It is noteworthy that the optimal feeding stroke E and the optimal swimming stroke D are qualitatively similar and have the same effective recovery structure, the main difference being the larger amplitude of the swimming stroke D.

Fig. 3 *C* and *F* represent the deformations induced by a single stroke A and E on an initially circular material line. The amplitude of deformations indicate that the breaststroke is creating a fluid flow at a larger scale than the undulatory stroke: The larger net volumetric flow rate toward the cell surface is consistent with larger feeding currents.

Stroke Kinematics and Nutrient Uptake. Although the feeding efficiency $\mathscr{E}_f$ is an accurate measure of the size of the feeding currents, it is not directly related to nutrient uptake. In order to compare the exact rates of nutrient uptake associated with the computed strokes, we solved the advection–diffusion equation around the cell for stroke E and, for comparison, strokes A and D:

$$\frac{\partial C}{\partial t} + \boldsymbol{u}\cdot\nabla C = D\nabla^2 C, \qquad [4]$$

where C is the three-dimensional time-dependent nutrient concentration field around the swimmer. We imposed a perfect absorption boundary condition at the surface S of the cell $C(r = R) = 0$ and a prescribed concentration distribution at infinity C_∞. The velocity field $\boldsymbol{u}$ around the biflagellated swimmer depends on the specifics of the swimming gait and is computed numerically from the known deformations of the optimal strokes (see *Methods*). Nutrient uptake is characterized by the nutrient transfer rate, or flux, at the surface S of the cell $F = -\langle \iint_S D(\partial C/\partial r)dS\rangle$, where the brackets indicate that the flux is averaged over one stroke period. Both the concentration field C and the flux F strongly depend on the relative size of the advection term in Eq. **4** and hence on the Péclet number Pe.

In addition to Pe^U (Eq. **2**), which characterizes the swimming velocity U, we define an alternative Péclet number based on the mechanical power ϕ as

$$\mathrm{Pe}^\phi = \frac{U_\phi R}{D}, \qquad [5]$$

where U_ϕ is the characteristic velocity associated with the mechanical power defined earlier. From Eq. **1**, we find $\mathrm{Pe}^\phi = \mathrm{Pe}^U/\sqrt{\mathscr{E}_s}$. Given that $\mathscr{E}_s \sim 0.001$–0.008, Pe^ϕ is typically 10–30 times larger than Pe^U depending on the stroke considered. Strokes performed at equal Pe^U (Eq. **2**) produce the same swimming velocity U, whereas strokes performed at equal Pe^ϕ (Eq. **5**) consume the same mechanical power ϕ and thus have the same energetic cost. All simulations were started from an equilibrium concentration field at time $t = 0$ with no advective background flow. We focused our attention on previously computed optimal strokes which have been observed experimentally, namely: the undulatory stroke A and the effective recovery strokes D and E.

We first considered the case of a constant concentration field at infinity, C_∞. We computed the unsteady concentration field C and the flux F numerically over several stroke periods. The time-dependent concentration field C went through an initial transient mode, during which the average nutrient flux increased from the diffusive value $F(\mathrm{Pe} = 0)$ to a constant steady-state value $F(\mathrm{Pe})$. Fig. 4*A* represents snapshots of the oscillatory steady-state concentration fields during one period of strokes A and E. In both cases, the effect of the advection term in Eq. **4** can be readily seen from the deformations of the initially spherical isoconcentration surfaces. The distortions of the concentration field are more severe for the breaststroke than for the undulatory stroke, which allows stroke E to generate larger concentration gradients at the surface of the sphere leading to an increased nutrient uptake. The advective enhancement of the nutrient transfer rate is best represented by the Sherwood number (Sh) as a function of the Péclet number

$$\mathrm{Sh}(\mathrm{Pe}) = 2\frac{F(\mathrm{Pe})}{F(\mathrm{Pe} = 0)}. \qquad [6]$$

The Sh reflects the increase in the nutrient flux due to advection once the flux has reached its steady-state value $F(\mathrm{Pe})$. For each stroke, we find Sh to increase with both Pe^U and Pe^ϕ (Fig. 4 *B* and *C*) in agreement with previous studies (5, 7). At a given swim-

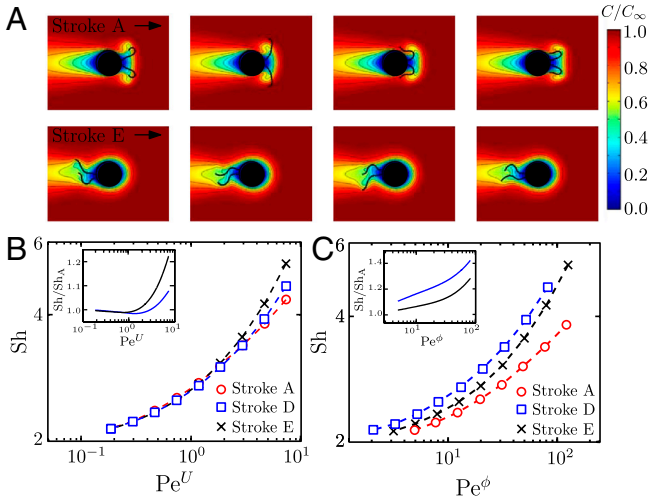

Fig. 4. (*A*) Snapshots of the nutrient concentration fields around a model swimmer for $\mathrm{Pe}^U = 7$ at successive times computed by solving Eq. **4** numerically. The top row corresponds to the undulatory stroke A, which we computed as a local optimal for $\mathscr{E}_s$ and the bottom row to the breaststroke E, which is the optimal stroke found for $\mathscr{E}_f$. (*B*) Loglog plot of Sh versus $\mathrm{Pe}^U = 7$. The inset corresponds to a semilogarithmic plot of the ratio of Sh computed for stroke D and E divided by Sh for stroke A as a function of $\mathrm{Pe}^U = 7$. (*C*) Loglog plot of Sh versus Pe^ϕ. The inset corresponds to a semilog plot of $\mathrm{Sh}/\mathrm{Sh}_A$ versus Pe^ϕ.

ming velocity U corresponding to $\mathrm{Pe}^U = 1$, Sh is 1.5% higher for the breaststroke E than for the undulatory stroke A and the increase reaches 25% at $\mathrm{Pe}^U = 7$ (Fig. 4*B*). Over the equivalent range of Pe^ϕ, Sh is 6% higher for stroke E and 15% higher for stroke D compared to the undulatory stroke A at $\mathrm{Pe}^\phi = 10$. This increase reaches 28% for stroke E and 44% for stroke D at $\mathrm{Pe}^\phi = 70$ (Fig. 4*C*).

Next we examined the case of a swimmer moving in a gradient of nutrient concentration. We solved Eq. **4** for a swimmer traveling at a prescribed Pe^U aligned with a constant gradient of concentration $[\nabla C]_\infty$ such that $C(x,y = \pm\infty, z = \pm\infty) = [\nabla C]_\infty x$, with $x = 0$ at the initial position of the center of the cell. For each stroke, A, D, and E, we computed the time-dependent concentration field C over several stroke periods and evaluated the nutrient flux $F(x)$ as the swimmer moved in the $\hat{\boldsymbol{x}}$ direction.

To determine how effectively the kinematics transmit information about the concentration field to the cell, we quantify how closely the value of the nutrient flux follows the level of the background concentration field at infinity. Consequently, we defined a dimensionless nutrient flux $\mathscr{F}$

$$\mathscr{F}\left(\frac{x}{R}\right) = \frac{F(x)}{F(\mathrm{Pe}^U)}. \qquad [7]$$

The denominator $F(\mathrm{Pe}^U)$ is the previously computed steady-state value of the nutrient flux for the same stroke performed at the same Pe^U but in a constant uniform concentration field at infinity $C_\infty = (\nabla C)_\infty \cdot R$. The value of the nondimensional flux $\mathscr{F}$ is expected to be related to the nondimensional background concentration level at infinity, which is linear in the position x along $\hat{\boldsymbol{x}}$ and equal to x/R. In the diffusive case $\mathrm{Pe}^U = 0$, the nutrient flux scales exactly with the concentration at infinity, regardless of the stroke kinematics and $\mathscr{F}(\frac{x}{R}) = \frac{x}{R}$. In this situation, the nutrient flux precisely reflects the concentration at infinity and provides the organism with an exact measure of the nutrient levels as it moves in the gradient field. For finite Pe^U, the effect of the specific stroke kinematics on the advection of nutrient becomes significant and affects how closely $\mathscr{F}$ follows the concentration field (Fig. 5*A*). It bears emphasis that for $\mathscr{F}(x/R) \geq x/R$, the value of $\mathscr{F}$ is characteristic of a nondimensional concentration level at a coordinate x/R greater than the actual position of the swimmer. In other words, the nutrient flux provides an anticipated measure of the concentration field. Conversely if $\mathscr{F}(x/R) \leq x/R$, the nutrient flux carries a delayed measure of the concentration at infinity. For swimmers advancing at equal velocity, we found that $\mathscr{F}(x/R) \geq x/R$ for breaststrokes, whereas $\mathscr{F}(x/R) \leq x/R$ for the undulatory stroke. Hence the breaststroke E enhances sensing of the nutrient concentration as the organism moves in the gradient field, whereas the undulatory stroke A delays transfer of information (Fig. 5*A*).

This result is corroborated, when considering variations in flux. We computed $\nabla\mathscr{F}$ as the derivative of $\mathscr{F}$ with respect to x/R. For $\mathrm{Pe}^U = 0$, $\nabla\mathscr{F} = 1$ and the constant gradient in flux carries exact information of the constant gradient in concentration $(\nabla C)_\infty$, regardless of the stroke kinematics. At finite Pe^U, $\nabla\mathscr{F}$ is no longer exactly equal to 1, but rather converges to the steady-state value $\nabla\mathscr{F} \to 1$ after a transient regime. At these transitional values $\mathrm{Pe}^U \sim 1$–10, the details of the stroke kinematics become relevant, affecting the time required for a cell sensing gradients in nutrient flux to perceive accurately the concentration gradient at infinity. Our results indicate that the transient is very short for the breaststrokes D and E but much longer for the undulatory stroke A (Fig. 5*B*).

Discussion

The beating patterns of biflagellated phytoplankon have been investigated experimentally in the context of flagellar synchronization and the motile response to chemical and light signals (8, 10–13). Recent experimental work demonstrated the effective exploitation of microscale resource patches by marine microorganisms (2) and by phytoplankton in particular (23). The ability

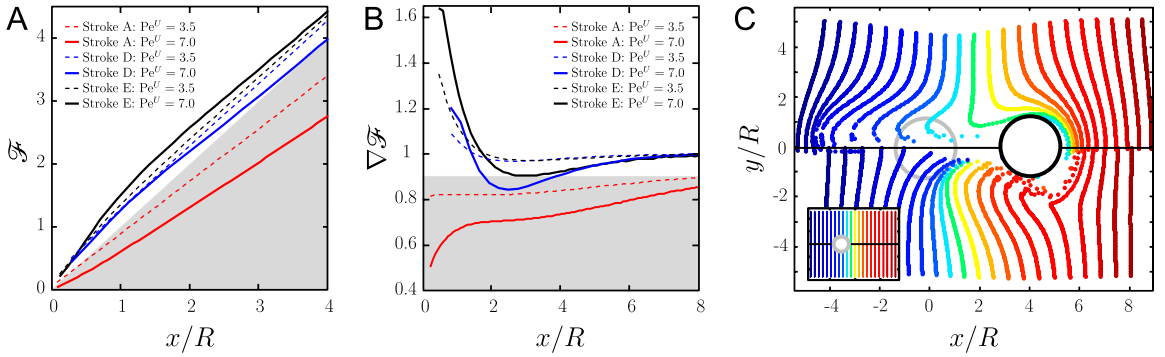

Fig. 5. (*A*) Nondimensional flux $\mathscr{F}$ as a function of the nondimensional position of the swimmer along the $\hat{\boldsymbol{x}}$ axis x/R. Shaded area corresponds to $\mathscr{F}(x/R) \leq x/R$. (*B*) Derivative of $\mathscr{F}$ as a function of x/R. Shaded area corresponds to $\nabla\mathscr{F} < 0.9$. (*C*) Advection of material particles induced by stroke A (*Upper*) and stroke E (*Lower*) after the swimmer has traveled a distance $x/R = 4$. Inset represents the location of the material particle at the initial time.

to take advantage of such microscale patches (micrometer through millimeter) before they dissipate relies on a rapid chemotactic response (1, 2, 23), which can be improved both through effective locomotion and through the generation of feeding currents around the cell. We have determined—by defining relevant swimming ($\mathscr{E}_s$) and feeding ($\mathscr{E}_f$) efficiencies, which we used as objective functions to find optimal stroke patterns—that the observed flagellar stroke patterns of unicellular phytoplanktons are optimized for both locomotive and feeding functions.

We have found four local optima for $\mathscr{E}_s$ and one optimum for $\mathscr{E}_f$ (Fig. 2). All but one of these stroke kinematics have been observed experimentally in living organisms (8, 10–13). In particular, the qualitative agreement between our computed optimal undulatory and breaststrokes A, D, E, and experimentally recorded images is striking (Fig. 3). These similarities suggest that hydrodynamics is the dominant factor in determining the organization of the stroke. It also bears emphasis that the only computed kinematics *not* observed experimentally, stroke C, is the only stroke for which regions of high curvature are initiated at both ends of the flagellum (rather than solely at the base) and travel in opposite directions simultaneously. This observation suggests a possible physiological limitation to stroke patterns of eukaryotic flagella, whereby bending can only be induced at the base and travel toward the tip.

Both the undulatory and the breaststroke are found to be locally optimal for the swimming efficiency (Fig. 2). Free swimming *Chlamydomonas* cells have been observed to swim considerably faster using the breaststroke $U^{\mathrm{D}} = 150 \pm 50$ μm·s^{-1} (10, 24) rather than the undulatory stroke $U^{\mathrm{A}} = 50$ μm·s^{-1} (12). Our theoretical results agree with these observations as the swimming efficiency of the optimal breaststroke D, $\mathscr{E}_s^{\mathrm{D}} = 0.0080$, is significantly higher than that of the optimal undulatory stroke $\mathscr{E}_s^{\mathrm{A}} = 0.0014$. These values for $\mathscr{E}_s$ also agree quantitatively with the measured values for the swimming velocities. The velocity ratio between stroke D and A can be expressed theoretically from Eq. **1** as $U^{\mathrm{D}}/U^{\mathrm{A}} = \sqrt{\mathscr{E}_s^{\mathrm{D}}\phi^{\mathrm{D}}/\mathscr{E}_s^{\mathrm{A}}\phi^{\mathrm{A}}}$. Assuming the rate of work ϕ exerted by *Chlamydomonas* to be independent of the particular stroke executed, we can predict the velocity ratio theoretically $U^{\mathrm{D}}/U^{\mathrm{A}} = \sqrt{\mathscr{E}_s^{\mathrm{D}}/\mathscr{E}_s^{\mathrm{A}}} = 2.4$, which compares favorably with experimental measurements $U^{\mathrm{D}}/U^{\mathrm{A}} = 3 \pm 1$. Additionally, our computed breaststroke D travels a distance of 1.4 μm per stroke and the undulatory stroke A travels 0.4 μm per stroke. Given the typical beating frequencies of 40–64 Hz reported for the breaststroke (10) and 80 Hz reported for the undulatory stroke (12), our model predicts a swimming velocity of ≈56–90 μm·s^{-1} for the breaststroke and ≈32 μm·s^{-1} for the undulatory stroke. These predicted values are comparable, albeit somewhat lower, than the velocities measured experimentally. The discrepancy is likely to be due to our assumption of a spherical head, for which the viscous drag is significantly higher than for a cell of aspect ratio 0.5–0.6, as it is the case in these experimental studies.

The values of $\mathscr{E}_s$ computed for our model biflagellated swimmer can be compared with those computed for uniflagellated swimmers (17), whose strokes have been optimized for swimming efficiency. For uniflagellated swimmers with a spherical head of diameter $R = 5$ μm, the value of $\mathscr{E}_s$ depends on the length of the flagellum and reaches a maximum of 0.0140 (17) for a flagellum of length $L = 120$ μm. This observation indicates that the particular biflagellated geometry investigated here does not gain anything in swimming efficiency over uniflagellated organisms.

Consequently, we investigated optimal stroke patterns in relation to another function, namely feeding and enhancement of nutrient uptake via the generation of feeding currents. In this spirit, we derived the expression for the feeding efficiency $\mathscr{E}_f$, which characterizes the magnitude of the volumetric inbound flux toward the surface of the swimmer induced by a stroke performed at a given rate of work. Using $\mathscr{E}_f$ as an objective function, our optimization procedure always converged to a breaststroke E (Fig. 2*E*), qualitatively similar to experimental observations (Fig. 3), and which only differed from the swimming breaststroke D in amplitude. Visualizing and comparing the deformations induced by a single stroke on a material line confirms that the breaststroke creates a flow around the cell on a larger scale than the undulatory stroke and draws fluid closer to the surface of the cell more effectively (Fig. 3).

In order to quantify precisely how the stroke kinematics impact nutrient uptake, we solved the full advection–diffusion equation given the optimal kinematics and compared the values of the nutrient flux at the surface of the swimmer. We found that the effect of the specific stroke patterns on nutrient flux becomes significant for transitional values of the Péclet number $\mathrm{Pe}^U \sim 1$–10, on the same order as the characteristic Péclet number exhibited by *Chlamydomonas*. In a constant concentration field at infinity, the swimming breaststroke D generates a nutrient flux 44% higher than the undulatory stroke performed at equal energetic cost $\mathrm{Pe}^\phi = 70$ and the feeding breaststroke E creates a flux 25% higher than the undulatory stroke performed at equal swimming velocity $\mathrm{Pe}^U = 7$. These results demonstrate the crucial role of stroke kinematics in increasing the rate of nutrient uptake and show that, in the transitional Péclet number regime, the breaststroke is better than the undulatory stroke at enhancing nutrient uptake via the creation of feeding currents.

We also examined the effectiveness of stroke kinematics in transmitting information about the concentration field to the cell surface, by investigating how closely the variations in nutrient flux follow the variations in the concentration field. For a constant gradient at infinity, the levels of both the nutrient flux $\mathscr{F}$ and its gradient $\nabla\mathscr{F}$ indicate that the breaststroke conveys an anticipated measure of the concentration landscape, whereas the undulatory stroke delays the transfer of information. This observation can be rationalized by considering the displacement of material particles induced by the different stroke kinematics. In Fig. 5*C*, it becomes apparent that, with the breaststroke, the organism tends to pull the fluid in the front toward its surface, providing information on the field ahead. The undulatory stroke on the other hand, tends to push away the fluid in the front, hence delaying the transmission of information about the upcoming conditions. The variations of $\nabla\mathscr{F}$ as the cell advances best characterize how fast changes in the background concentration field can be sensed at the cell surface. For all stroke kinematics, $\nabla\mathscr{F}$ eventually converges to a constant steady-state $\nabla\mathscr{F} = 1$ after going through a transient. The duration of this transient is strongly dependent on the stroke kinematics. For $\mathrm{Pe}^U = 7$, we found the response time at which $\nabla\mathscr{F}$ reached 90% of its steady-state value to be $x/U \sim R/U$ for the breaststroke but up to $x/U \sim 10R/U$ for the undulatory stroke. Hence, although the breaststroke allows the organism to sense the concentration gradient accurately after swimming a distance of only ∼5 μm, the undulatory stroke requires swimming a distance of ∼50 μm to acquire the same information. The difference between these response lengths is significant considering that phytoplankton have been shown to take advantage of nutrient patches a small as 100 μm (23). In addition, it is noteworthy that during the transient $\nabla\mathscr{F} > 1$ for the breaststroke, which provides an amplified measure of the concentration gradient, while $\nabla\mathscr{F} < 1$ for the undulatory stroke, which initially damps the concentration gradient (Fig. 5*B*). This improved sensing associated with the breaststroke favorably affects the speed of the chemotactic response and may improve the ability of an organism to detect and take advantage of nutrient patches.

Methods

Hydrodynamics. The hydrodynamics in our system is governed by the Stokes equations. These are solved using a singularity method, in which fundamental solutions to the Stokes equations are distributed along the centerline of both flagella and at the center of the spherical head, such that the no-slip

boundary condition is satisfied to first order along the surface of the deforming body. The system of fundamental solutions required to represent the head and the slender tail can be found, respectively, in refs. 25 and 26. Hydrodynamic interactions between the head and the tail are taken into account by using Faxén's laws (27). In this formulation, the hydrodynamics is governed by an integral equation in the singularity distribution. The tail is discretized into a regular grid of N elements (typically $N \approx 100$) and the integral equation is solved numerically using a midpoint collocation scheme to find the motion of the swimmer. Additionally, the flow field $\boldsymbol{u}$ at each point around the swimmer can be computed by integrating the contribution to the flow of each singularity over the entire distribution.

Optimization. Optimal strokes are computed using the MATLAB `fmincon()` routine, which implements sequential quadratic programming to find optimal values of a nonlinear function subject to constraints. Such nonlinear programming algorithms require a parameterization of the stroke kinematics via a finite set of parameters representing the periodic time variation of the curvature $\gamma(t,s)$. Here, we impose the curvature at a discrete set N_γ of nodes along the tail (typically $N_\gamma \approx 25$). At each of these nodes, the curvature is discretely represented by its first Fourier modes. The curvature at the N elements of the spatial discretization of the tail is deduced by cubic spline interpolation. This parameterization of the curvature $\gamma(s,t)$ is general and can represent any periodical deformation of the swimmer. Strokes are optimized subject to the constraint that the swimming path remains straight and that it does not generate net rotation.

Feeding Efficiency. The feeding efficiency, $\mathscr{E}_f$, depends on the characteristic length scale ℓ of fluid displaced, which we define by considering the displacement of material particles in the $(\hat{\boldsymbol{x}}, \hat{\boldsymbol{y}})$ plane containing both flagella (Fig. 1). Let $\boldsymbol{r}_0(\theta,t)$ represent a closed material line in the $(\hat{\boldsymbol{x}}, \hat{\boldsymbol{y}})$ plane, with θ the polar angle from the $\hat{\boldsymbol{x}}$ axis and t denoting time. At $t = 0$, the material line corresponds to a circle of radius $|\boldsymbol{r}_0(\theta,0)| = 2R$ around the cell (Fig. 3 *C* and *F*). Following the motion of material points, we track the deformation of this material line, which after one stroke period $\tau = 1/f$ is described by $\boldsymbol{r}_0(\theta,\tau)$. The surface area of the domain, A, is defined as points of polar coordinates (r, θ) in the $(\hat{\boldsymbol{x}}, \hat{\boldsymbol{y}})$ plane which satisfy both $r \le |\boldsymbol{r}_0(\theta,0)|$ and $r \ge |\boldsymbol{r}_0(\theta,\tau)|$ (Fig. 3 *C* and *F*). This area A corresponds to material points dragged closer to the cell surface during the stroke and is a measure of the volumetric flow rate. The characteristic length scale ℓ of displaced fluid is defined as $\ell = \sqrt{A}$.

Numerical Solver for the Advection–Diffusion Equation. The time-dependent advection–diffusion Eq. **4** is solved numerically using finite differences. We used a spherical coordinate system replacing the radial distance coordinate r with $\xi = \ln r$ in order for mesh points to be more densely packed at the surface of the sphere. The boundary condition on the concentration field at infinity C_∞ is imposed at $r = 300R$.

ACKNOWLEDGMENTS. This work was partially supported by National Science Foundation Grant CCF-0323672 and CTS-0624830..

1. Fenchel T (2002) Microbial behavior in a heterogeneous world. *Science* 296:1068–1071.
2. Stocker R, Seymour JR, Samadani A, Hunt DE, Polz MF (2008) Rapid chemotactic response enables marine bacteria to exploit ephemeral microscale nutrient patches. *Proc Natl Acad Sci USA* 105:4209–4214.
3. Nicastro D, et al. (2006) The molecular architecture of axonemes revealed by cryoelectron tomography. *Science* 313:944–948.
4. Short M-B, et al. (2006) Flows driven by flagella of multicellular organisms enhance long-range molecular transport. *Proc Natl Acad Sci USA* 103:8315–8319.
5. Magar V, Goto T, Pedley T-J (2003) Nutrient uptake by a self-propelled steady squirmer. *Q J Mech Appl Math* 56:65–91.
6. Magar V, Pedley T-J (2005) Average nutrient uptake by a self-propelled unsteady squirmer. *J Fluid Mech* 539:93–112.
7. Langlois V-J, Andersen A, Bohr T, Visser A-W, Kiorboe T (2009) Significance of swimming and feeding currents for nutrient uptake in osmotrophic and interception-feeding flagellates. *Aquat Microb Ecol* 54:35–44.
8. Polin M, Tuval I, Drescher K, Gollub J-P, Goldstein R-E (2009) *Chlamydomonas* swims with two "gears" in a eukaryotic version of run-and-tumble locomotion. *Science* 325:487–490.
9. Durham W-M, Kessler J-O, Stocker R (2009) Disruption of vertical motility by shear triggers formation of thin phytoplankton layers. *Science* 323:1067–1070.
10. Rüffer U, Nultsch W (1985) High-speed cinematographic analysis of the movement of *Chlamydomonas*. *Cell Motil Cytoskeleton* 5:251–263.
11. Rüffer U, Nultsch W (1991) Flagellar photoresponses of *Chlamydomonas* cells held on micropipiettes: II. Change in flagellar beat pattern. *Cell Motil Cytoskeleton* 18:269–278.
12. Rüffer U, Nultsch W (1995) Flagellar photoresponses of *Chlamydomonas* cells held on micropipiettes: III. Shock response. *Bot Acta* 108:255–265.
13. Yoshimura K, Shingyoji C, Takahashi K (1997) Conversion of beating mode in *Chlamydomonas* flagella induced by electric stimulation. *Cell Motil Cytoskeleton* 36:236–245.
14. Purcell EM (1997) The efficiency of propulsion by a rotating flagellum. *Proc Natl Acad Sci USA* 94:11307–11311.
15. Becker LE, Koehler SA, Stone HA (2003) On self-propulsion of micro-machines at low Reynolds number: Purcell's three-link swimmer. *J Fluid Mech* 490:15–35.
16. Tam D, Hosoi AE (2007) Optimal stroke patterns for Purcell's three-link swimmer. *Phys Rev Lett* 98:068105.
17. Tam D (2008) Motion at low Reynolds number. PhD thesis (MIT Press, Cambridge, MA).
18. Graham LE, Graham JM, Wilcox LW (2008) *Algae Second Edition* (Benjamin Cummings, San Francisco), pp 486–546.
19. Govorunova EG, Sineshchekov OA (2005) Chemotaxis in the green flagellate alga *Chlamydomonas*. *Biochemistry (Mosc)* 70:869–879.
20. Pepper RE, Roper M, Ryu S, Matsudaira P, Stone HA (2010) Nearby boundaries create eddies near microscopic filter feeders. *J R Soc Interface* 7:851–862.
21. Higdon JJL (1979) The generation of feeding currents by flagellar motions. *J Fluid Mech* 94:305–330.
22. Jiang H, Meneveau C, Osborn TR (1999) Numerical study of the feeding current around a copepod. *J Plankton Res* 21:1391–1421.
23. Seymour J-R, Marcos , Stocker R (2009) Resource patch formation and exploitation throughout the marine microbial food web. *Am Nat* 173:E15–29.
24. Weibel D-B, et al. (2005) Microoxen: Microorganisms to move microscale loads. *Proc Natl Acad Sci USA* 102:11963–11967.
25. Chwang A-T, Wu T-Y (1975) Hydromechanics of low-Reynolds-number flow. Part 2. Singularity method for Stokes flows. *J Fluid Mech* 67:787–815.
26. Keller J-B, Rubinow S-I (1976) Slender-body theory for slow viscous flow. *J Fluid Mech* 75:705–714.
27. Happel J, Brenner H (1983) *Low Reynolds Number Hydrodynamics* (Martinus Nijhoff Publishers, The Hague), pp 226–227.